

# Supramolecular Structure of Membrane-Associated Polypeptides by Combining Solid-State NMR and Molecular Dynamics Simulations

Markus Weingarth,<sup>†</sup> Christian Ader,<sup>†</sup> Adrien J. S. Melquiond,<sup>†</sup> Deepak Nand,<sup>†</sup> Olaf Pongs,<sup>‡</sup> Stefan Becker,<sup>§</sup> Alexandre M. J. J. Bonvin,<sup>†</sup> and Marc Baldus<sup>†\*</sup>

<sup>†</sup>Bijvoet Center for Biomolecular Research, Utrecht University, Utrecht, The Netherlands; <sup>‡</sup>Institut für Neurale Signalverarbeitung, Zentrum für Molekulare Neurobiologie der Universität Hamburg, Hamburg, Germany; and <sup>§</sup>Department of NMR-based Structural Biology, Max Planck Institute for Biophysical Chemistry, Göttingen, Germany

**ABSTRACT** Elemental biological functions such as molecular signal transduction are determined by the dynamic interplay between polypeptides and the membrane environment. Determining such supramolecular arrangements poses a significant challenge for classical structural biology methods. We introduce an iterative approach that combines magic-angle spinning solid-state NMR spectroscopy and atomistic molecular dynamics simulations for the determination of the structure and topology of membrane-bound systems with a resolution and level of accuracy difficult to obtain by either method alone. Our study focuses on the *Shaker B* ball peptide that is representative for rapid N-type inactivating domains of voltage-gated K<sup>+</sup> channels, associated with negatively charged lipid bilayers.

## INTRODUCTION

Membrane proteins and peptides play a crucial role in various biological pathways and represent major drug targets. Yet, only a small number of their tertiary structures have been determined to date, mainly due to the complexity to crystallize these systems in the presence of lipids (1). Magic-angle spinning (2) (MAS) solid-state NMR (ssNMR) spectroscopy allows studying membrane proteins and peptides in their native environment and thus gives access to both tertiary and quaternary structure (3–9) in close reference to protein function (10,11). For example, ssNMR-based structural studies were conducted on a variety of membrane-associating peptides (12,13), including channel-forming peptides (14,15), and served to establish intermolecular contacts between membrane-bound antimicrobial β-hairpin peptides (16). A particularly important aspect in such structural studies relates to the atomic level definition of the macroscopic orientation of proteins and the influence of lipid-peptide interactions in the lipid bilayer. Experimental ssNMR approaches to probe the supramolecular structure of membrane-embedded proteins have relied on H<sub>2</sub>O-edited ssNMR experiments (17–20), paramagnetic quenchers (21,22), H/D-exchange (23), selectively <sup>2</sup>H (24), or <sup>19</sup>F (25) labeled samples and, particularly, the measurements of <sup>13</sup>C and <sup>15</sup>N chemical-shift anisotropies in oriented samples (26).

Molecular dynamics (MD) simulations can give increasingly accurate insight into membrane-associated molecular systems but require taking into account that chosen starting conditions (27) may impact the MD results. Therefore, combined approaches have been introduced that correlate ssNMR observables with MD trajectories (27–36) to

enhance the general reliability of the results. For example, combining computational and experimental studies has aided the precise determination of helical tilt from PISA wheels or deuterium quadrupolar splitting (27,28,31,34,36,37). In addition, simulations have been used to complete the often sparse information delivered by ssNMR to study oligomerization of transmembrane helices, side-chain-lipid interactions (38), and the conformational space (29) and dynamics of membrane-associated peptides (39). Finally, MD simulations have been previously employed to validate ssNMR structures of amyloid fibrils (40) and the Gramicidin A channel (41).

Here, we propose a general approach to establish and refine the supramolecular structure of membrane-bound biomolecules by iterative application of MAS ssNMR experiments and MD simulations. Importantly, one uniformly <sup>13</sup>C, <sup>15</sup>N labeled sample suffices to characterize both structure and topology, i.e., the positioning of the polypeptide within the membrane. We used this approach to study the *Shaker B* (ShB) peptide bound to negatively charged lipid bilayers. The peptide belongs to a family of peptides conferring N-type inactivation to several ion channels, for instance the *Shaker B* K<sup>+</sup> channel. It comprises the first 20 residues of ShB and hence corresponds to the channel's N-type inactivation (ball) domain. The ball domain acts as an autoinhibitory channel blocker, a process of considerable pharmacological relevance (42). Although liquid-state NMR studies showed that the isolated peptide is unstructured in solution (43), biophysical investigations suggested the monomeric ShB peptide to bind to negatively charged lipid bilayers adopting a β-strand secondary structure (44,45). This is remarkable, because in contrast to α-helical backbone conformations, which are typically observed for membrane-associated peptides, every second polar backbone position remains unsaturated in an isolated

Submitted February 28, 2012, and accepted for publication May 7, 2012.

\*Correspondence: m.baldus@uu.nl

Editor: Mei Hong.

© 2012 by the Biophysical Society  
0006-3495/12/07/0029/9 \$2.00

doi: 10.1016/j.bpj.2012.05.016

$\beta$ -strand. Notably, such a  $\beta$ -strand conformation has also been hypothesized for the channel-bound peptide, implying that the open K<sup>+</sup> channel and the lipid bilayer provide a molecular binding environment of comparable characteristics, namely a hydrophobic setting and a negative surface potential (44,46). To date, there is no detailed structural data for the inactivating peptide of ShB bound to the channel pore or lipid bilayers. In the following, we demonstrate that the tailored combination of ssNMR and MD provides a means to dissect the remarkable interplay between intra- and intermolecular interactions that stabilize its supramolecular structure in a membrane setting.

## MATERIALS AND METHODS

### Sample preparation

The coding sequence of the ShB peptide was cloned into a modified pMal vector (New England Biolabs, Frankfurt am Main, Germany). The (<sup>13</sup>C, <sup>15</sup>N) labeled maltose-binding protein fusion protein was expressed in M9 minimal medium with <sup>13</sup>C6-D-glucose (Eurisotop, Saint-Aubin, France) and <sup>15</sup>NH<sub>4</sub>Cl (Sigma Aldrich, St. Louis, MO) as the sole <sup>15</sup>N and <sup>13</sup>C sources, respectively. The fusion protein was purified on a Nickel Sepharose HiTrap column (GE Healthcare, Chalfont, St Giles, UK) and cleaved with tobacco etch virus protease. The released ShB peptide was further purified by reversed phase HPLC. The purity of the peptide was confirmed by electrospray ionization mass spectrometry. For reconstitution with liposomes 1.95 mg of (<sup>13</sup>C, <sup>15</sup>N) ShB peptide was dissolved in reconstitution buffer (100 mM sodium citrate, pH 4.0, 4 mM *n*-decyl- $\beta$ -D-maltopyranoside (Calbiochem, San Diego, CA)). Next, 6.58 mg of Diacylphosphatidylcholine and 5.39 mg of bovine heart Cardiolipin (Avanti Polar Lipids, Alabaster, AL) (7:3, mol/mol), corresponding to a 13.7 lipid/peptide ratio (mol/mol), were dissolved in chloroform/methanol (1:1, v/v) and a lipid film was generated by evaporation in a nitrogen stream. The film was dissolved in reconstitution buffer, sonicated for 10 min, combined with the peptide solution, and incubated for 2 h. The detergent was removed by incubation with Calbiosorb resins (Calbiochem). The liposomes were pelleted by ultracentrifugation at 134,000  $\times$  g for 1 h at 4°C. The liposome pellet was washed with 100 mM sodium citrate pH 4.0. Finally, the pellet was transferred into a 3.2 mm MAS rotor.

### Solid-state NMR spectroscopy

All ssNMR experiments were conducted using 3.2 mm probeheads at magnetic fields of 11.7 and 16.4 T corresponding to 500 and 700 MHz <sup>1</sup>H frequencies, respectively. Unless stated otherwise, the MAS frequency was set to 13 kHz (16.4 T) and 10 kHz (11.7 T) and SPINAL64 decoupling (47) was employed during acquisition. The effective sample temperature ranged from 277 to 283 K. <sup>13</sup>C and <sup>15</sup>N resonances were calibrated using adamantane and the tripeptide AGG (48) as external references, respectively. Sequential <sup>15</sup>N-<sup>13</sup>C resonance assignments were obtained from chemical-shift selective two-dimensional NC $\alpha$  and NC' correlation spectra (49) in conjunction with <sup>13</sup>C-<sup>13</sup>C correlation experiments performed under weak coupling conditions (50). Two-dimensional N/CHC (51) and PARIS-xy (52) experiments provided distance constraints. The PARIS-xy method ( $m = 2$ , recoupling amplitude 10 kHz, 250 ms mixing time) was applied at 500 MHz <sup>1</sup>H frequency and 13.9 kHz MAS frequency using PISSARRO (53) decoupling. Water-protein and lipid-protein interactions were probed employing T<sub>2</sub> filtered HHC correlation experiments (17–20). The <sup>1</sup>H T<sub>2</sub> filter was applied for a duration of 2 ms and <sup>1</sup>H-<sup>1</sup>H mixing times ranged between 0 and 4 ms. Details on the analyzed spectra are provided in Table S1 in the Supporting Material. Spectra were processed and peak inte-

grals were obtained using the software TopSpin 2.1 (Bruker Biospin, Germany). Spectra were analyzed using Sparky 3.114 (Goddard and Kneller, University of California, CA).

### Structure calculation

The structure of membrane-bound ShB peptide was determined by simulated annealing in the CNS (54) system starting from an extended conformer of the ShB peptide. Rigid body rotation of the ShB ssNMR structure and computation of correlation coefficients was implemented using the software MATLAB (The MathWorks, Natick, MA). The structures were visualized using PyMol 0.97 (DeLano Scientific LLC,). An ShB peptide-bilayer model was generated by orienting the ShB peptide according to the ssNMR data within an 1-palmitoyl-2-oleoyl-sn-glycero-3-phosphoglycerol (POPG) lipid bilayer obtained from MD simulations (55).

### Molecular dynamics simulations

All simulations were carried out using the GROMACS simulations package version 4.5.3 (56) with the GROMOS53a6 force field (57) and the Berger lipid parameters (58). The initial coordinates and topologies of an equilibrated 128-lipid POPG bilayer were obtained from Kukol (55). POPG was chosen because no GROMOS53a6 topology file for Cardiolipin was available at the time of this study. Note that the only known prerequisite for membrane insertion of the ShB peptide is the presence of negatively charged lipids (44–46). The ssNMR structure was placed into this bilayer with the orientation and insertion depth derived from T<sub>2</sub>-edited HHC experiments, referred to as ssNMR topology in this text. The lipids were subsequently expanded in the transversal plane and recompressed using the inflateGRO (59) methodology to pack the lipids around the peptide. The system was compressed to a final lipid surface of 70 Å<sup>2</sup> (55) and solvated with SPC water. Sodium ions were added to neutralize the system. The final system consisted of one ShB peptide, 127 lipids, 4905 water molecules, and 124 Na<sup>+</sup> ions. The system was equilibrated for 100 ps in an NVT-ensemble using a modified Berendsen thermostat (60). Throughout all MD simulations, the temperature was kept constant at 290 K (61). Sodium ions and water molecules were jointly coupled to the thermostat. The system was then equilibrated for 1 ns in an NPT-ensemble using the Nosé-Hoover thermostat (62) and semianisotropic Parrinello-Rahman pressure coupling. A production run was performed for 330 ns with a time step of 1 fs. The PME (63) method was used for the long-range electrostatic forces. The LINCS algorithm (64) was applied to constrain the bond lengths of the peptide and lipids, and the SETTLE algorithm was used to constrain water molecules. The stability and the phase of the bilayer over the course of simulations were evaluated by measuring the lipid density (Fig. S1) and the deuterium order parameters of the acyl chains (Fig. S2 and Fig. S3). Further MD simulations with different orientations of the peptide in the membrane were carried out for at least 20 ns each.

## RESULTS AND DISCUSSION

Our iterative joint approach of ssNMR experiments and MD simulations consists of the following steps: In a first round, a first guess of the structure of membrane-bound system and a first guess of the topology, which is essential to guide the MD simulations, are determined by dedicated ssNMR experiments for uniformly <sup>13</sup>C, <sup>15</sup>N labeled samples. The ssNMR structure and topology then serves as a starting point for atomistic MD simulations. These simulations are subsequently analyzed and new structurally important molecular contacts suggested by simulations are probed in a second

round using specifically tailored ssNMR experiments. This allows a validation (or rejection) of the structure. Once confirmed by the tailored ssNMR experiments, these new contacts are then used for another round of iterative structure determination. As a next step, orientation and insertion depth (i.e., the membrane topology) of the investigated system is refined by back-calculating an ssNMR observable (used to establish the initial topology) over the simulated trajectory. Finally, experimentally nontrivial parameters are investigated in simulated trajectories with experimentally cross-validated structure and topology. This yields a detailed picture of the supramolecular structure of the membrane-bound peptide or protein.

### Tertiary structure determination

To study the membrane-bound peptide by ssNMR, we reconstituted uniformly ( $^{13}\text{C}$ ,  $^{15}\text{N}$ ) labeled ShB peptide (Fig. 1 *a*) in negatively charged Dioleoylphosphatidylcholine/Cardiolipin lipid bilayers. Spectral assignments were obtained using a series of dipolar-based  $^{15}\text{N}-^{13}\text{C}$  and  $^{13}\text{C}-^{13}\text{C}$  correlation experiments (Fig. 1 *b*) (65). We obtained complete ( $^{13}\text{C}$ ,  $^{15}\text{N}$ ) resonance assignments for residues 1 through 12 of the ShB peptide (Table S2) consistent with a well-defined structure. For residue 13–20, however, no sequential contacts and only a small number of ambiguous intraresidual correlations could be detected. Furthermore, although side chains of L18 and L19 are represented in dipolar-based spectra (Fig. S4), no signals

could be identified using through-bond experiments. Hence, the eight C-terminal residues of the ShB peptide did not adopt a defined structure and were characterized by restricted dynamics, presumably due to transient interactions of the positively charged tail with negatively charged lipid-headgroups (see below). Secondary chemical shifts computed for residues 1–12 (Fig. S5) indicated a  $\beta$ -strand secondary structure, which agrees well with previous studies by fluorescence and infrared spectroscopy (44,45). Direct structural information for the membrane-bound ShB peptide was obtained from NHHC (51) (Fig. 1 *c*) through-space ssNMR experiments confirming the  $\beta$ -strand structure (Table S3). We explored possible  $\beta$ -hairpin tertiary structures by probing long-range backbone distances by CHHC (51) (Fig. 1 *d*) experiments, indicating an in-register  $\beta$ -hairpin (Fig. 1 *e*), characterized by short backbone distances between A2 and G11 as well as V4 and G9. We initially assumed a  $\beta$ -type (66) VIII turn arrangement for residues G6 and L7. Subsequently, we used the obtained distance and dihedral-angle constraints (Table S4) for a simulated annealing-based structure determination (54). Fig. 2 *a* shows the superposition of the three lowest energy structures. We validated the structures based on the stereochemical quality of the ensemble (Table S5) and by back-calculating chemical shifts and comparing them to the experimental data (Fig. S6). Although the backbone of the ssNMR structure was well defined, information about the side chains, which are potential key players for protein-membrane anchoring, was lacking and many

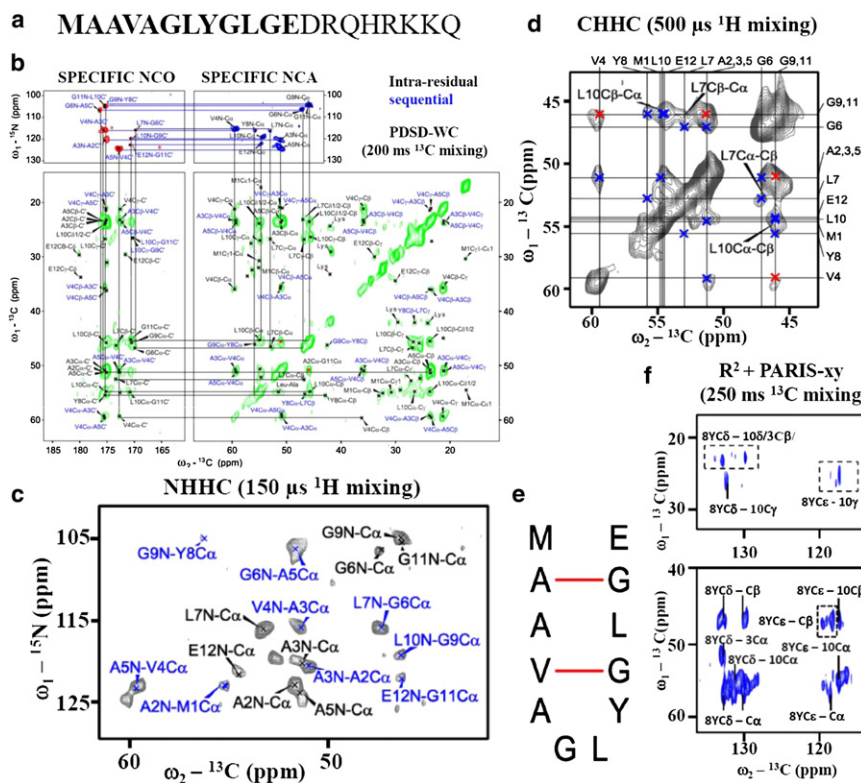


FIGURE 1 (a) Sequence of the ShB peptide. Residues with defined structure according to ssNMR are indicated in bold. (b) SPECIFIC NCOX (49) (red) and NCA (blue)  $^{15}\text{N}-^{13}\text{C}$  correlation spectra as well as PDSD  $^{13}\text{C}-^{13}\text{C}$  correlation spectra obtained under weak C $\alpha$ -C $\alpha$  recoupling (50) (green) showing intraresidual (black), sequential (blue), and interstrand (red) connectivity. (c) NHHC (51) spectrum recorded with a proton mixing time of 150  $\mu\text{s}$ . Intraresidue correlations are labeled black, sequential correlations blue. (d) C $\alpha$  region of a CHHC (51) spectrum employing 500  $\mu\text{s}$  proton mixing. Intraresidue crosspeaks are labeled and expected sequential crosspeaks are marked by blue crosses. Red crosses indicate long-range correlations expected for the  $\beta$ -hairpin shown in *e*: Potential  $\beta$ -hairpin of the ShB peptide. Expected long-range C $\alpha$ -C $\alpha$  and, accordingly, H $\alpha$ -H $\alpha$  contacts are indicated by red lines. (f) Spectrum of a PARIS-xy (52)  $^{13}\text{C}-^{13}\text{C}$  correlation experiment prompted by MD simulations. See online version for colored figure versions.

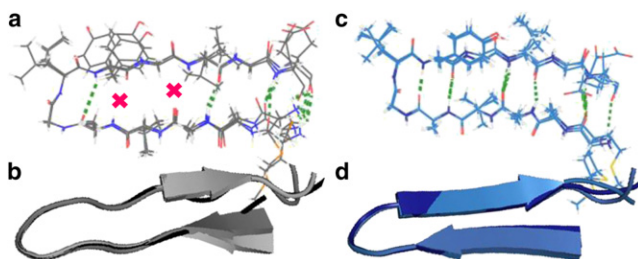


FIGURE 2 Comparison of (a and b) the ssNMR structure with (c and d) the ssNMR-MD structure. For the latter, eight new restraints were added (Table S6). The three lowest energy structures are superimposed. The inter- $\beta$ -strand hydrogen bonds are indicated as green dashed lines.

restraints, especially those for the ambiguous turn type, were solely based on chemical shifts, whose quantitative interpretation may be difficult in a membrane setting (67).

For these reasons, we aimed at refining the ssNMR structure using an iterative joint approach of ssNMR and atomistic MD simulations. Using the ssNMR structure and topology, which was determined by water-edited experiments and is discussed below, as starting structure, the ShB peptide was simulated over 330 ns in a solvated negatively charged racemic POPG membrane. We first investigated the quality of the ssNMR structure by comparing it with the trajectory of the simulated peptide. In very good agreement with the ssNMR data, the N-terminal residues 1–12 of membrane-bound ShB peptide formed a stable  $\beta$ -hairpin with a central turn formed by residues G6 and L7 over the timescale of the MD simulation, which is well reflected in the hydrogen bonding pattern (Fig. S7) and the Ramachandran plot (Fig. S8). In addition, the inter- $\beta$ -strand long-range contacts V4C $\alpha$ -G9C $\alpha$  and A2C $\alpha$ -G11C $\alpha$  are corroborated by the MD simulations (Fig. S7). Likewise, all short and long-range interproton contacts of the simulated ShB peptide agreed well with the ssNMR structure (Fig. S9). To further refine the ShB peptide structure, we probed additional intrapeptide contacts visible over the course of the trajectory using chemical-shift selective ssNMR experiments (52,68). From the MD trajectory, we observed the formation of a hydrophobic triad between the bulky Y8 and L10 side chains together with the A3 side chain of the opposite  $\beta$ -strand (Fig. S10). We examined the spatial proximity of these side chains experimentally using chemical-shift sensitive ssNMR sequences. We used combined transfer induced by rotational resonance (68) recoupling ( $n = 1$ ) and modulation sidebands (69) in one PARIS-xy experiment (52,70). With this approach, we could identify several long-range contacts between A3 and L10 to the aromatic moiety of Y8 (Fig. 1 f and Fig. S11) and could confirm the spatial proximity of residues V4 and G9 (Fig. S12), which was also observed in the CHHC spectrum (Fig. 1 d), validating the  $\beta$ -hairpin (Fig. 1 e). Furthermore, we experimentally observed multiple Y8C $\delta$  and Y8C $\epsilon$  resonances, suggesting different conformations of the side chain

of Y8, which will be discussed further below. We paid particular attention to the turn type formed by residues A5–Y8, which could not be elucidated unambiguously by ssNMR alone. In the MD simulations, the peptide almost immediately adopted a type II' turn, although the starting ssNMR structure featured a type VIII turn (Fig. S13). For the simulated peptide featuring type II' turn, the distance T8NH-L7H $\alpha$  is outstandingly long (3.3–3.7 Å), which is ~1 Å more than for the other sequential NH $i$ -H $\alpha$  $i+1$  contacts (Fig. S14), whereas all NH $i$ -H $\alpha$  $i+1$  distances are of similar range in the ssNMR structure. Indeed, the sequential contact NH $i$ -H $\alpha$  $i+1$  T8NH-L7H $\alpha$  was missing in NHHC experiments (Fig. 1 c), which together with the MD results strongly supports the formation of a type II' turn conformation. We also back-calculated the C $\alpha$  chemical shifts for residues 1–12 of the ssNMR structures and 20 MD structures using SPARTA+ (71) and compared them with experimental parameters (Fig. S6). For both structures, the chemical shifts of the  $\beta$ -strand residues 1–4 and 9–12 agreed well with the predicted values. Remarkably, the chemical shift predicted for residue V4C $\alpha$  on the basis of the ssNMR - MD structure was in better agreement with the experiment values than the prediction based on the ssNMR structure alone. We attribute this finding to the intra-peptide hydrogen bond between A2NH-V4H $\alpha$ , which could not be established by ssNMR alone. Indeed, the chemical shift of V4C $\alpha$  predicted for rare MD structures, for which this intrapeptide hydrogen bond did not occur, differed by ~2 ppm. Finally, we included all new restraints extracted from the MD trajectory and, except for the A2NH-V4H $\alpha$  hydrogen bond, validated by ssNMR (see Table S6).

## Topology determination

Information on topology of membrane-bound ShB peptide could be obtained by performing T<sub>2</sub>-edited HHC experiments (Fig. 3 a) (17–20). For short mixing times, magnetization transfer occurs in the initial rate regime, leading to correlations specific for water-peptide (e.g., residues M1 and E12) and lipid-peptide (e.g., V4 and G6) proximities. These data hence provided a basis to probe the macromolecular orientation of the peptide in the water/lipid bilayer environment. We determined crosspeak volumes for several resolved peptide resonances and calculated site-specific initial rates for water-protein and lipid-protein magnetization transfer (Fig. 3 b and Fig. S15). These data suggested that the  $\beta$ -hairpin intrudes the lipid bilayer with the hydrophobic turn pointing toward the core of the membrane, which is in good agreement with a tyrosine fluorescence study (45). We analyzed the transfer data by computing relative distances of the investigated spins to the water/bilayer interface. The ShB peptide structure, treated as rigid body, was then gradually reoriented with respect to the bilayer normal (Fig. S16), and we calculated correlation coefficients between these orientation-dependent restraints and

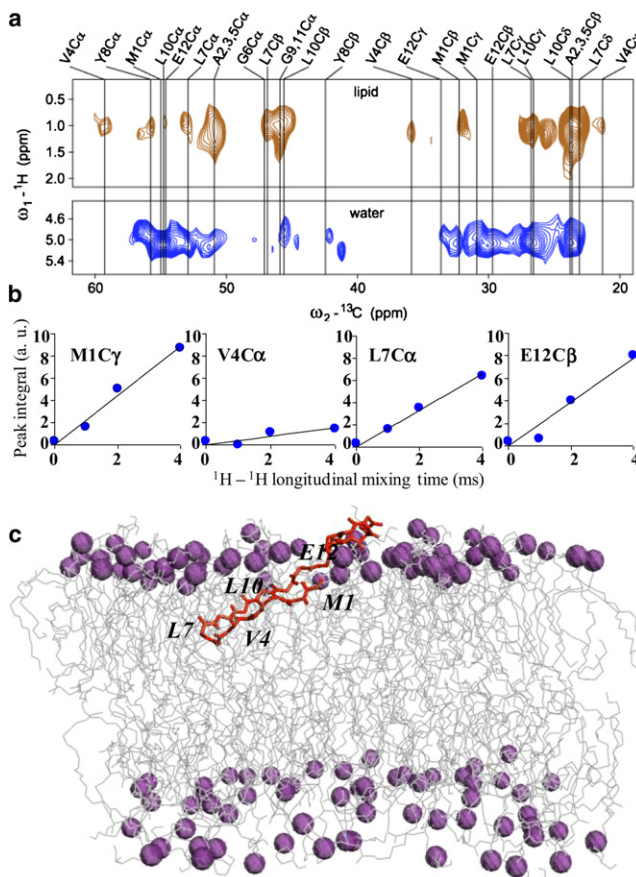


**FIGURE 3** Membrane topology of the ShB peptide obtained by ssNMR. (a)  $T_2$  filtered HHC spectrum obtained for a proton mixing time of 2 ms. Peptide resonances are indicated and lipid-protein and water-protein cross-peaks are colored brown and blue, respectively. Cross sections of lipid-peptide and water-peptide crosspeaks are shown in Fig. S15. (b) Integrals of water-protein (blue) crosspeaks computed from  $T_2$  filtered HHC spectra as a function of proton mixing time. (c) SsNMR topology of the ShB peptide. Phosphates are represented by spheres. See online version for colored figure versions.

the corresponding ratios of the initial rates for water-protein and lipid-protein transfer. The ssNMR membrane topology is then established as the topology that agrees best with all site-resolved transfer rates (Fig. 3 c).

In the next stage, this ssNMR topology was taken as a starting point and refined by back-calculating an ssNMR observable over the trajectory. In our case, this observable was the water access of spectrally resolved carbon resonances. The water access for each  $C\alpha$  of the N-terminal residues 1–12 was determined by back-calculating the number of water molecules within a radius of 9 Å averaged over the MD trajectory (Fig. S17) and compared with the experimentally determined backbone water access, which could be obtained for the  $C\alpha$  carbons of V4, G6, L7, and Y8 (Fig. 4 a). Remarkably, the water access of the peptide in the ssNMR-MD topology agreed very well with the experimental data. Note that this agreement of experimental and simulated water access was independent of variations in

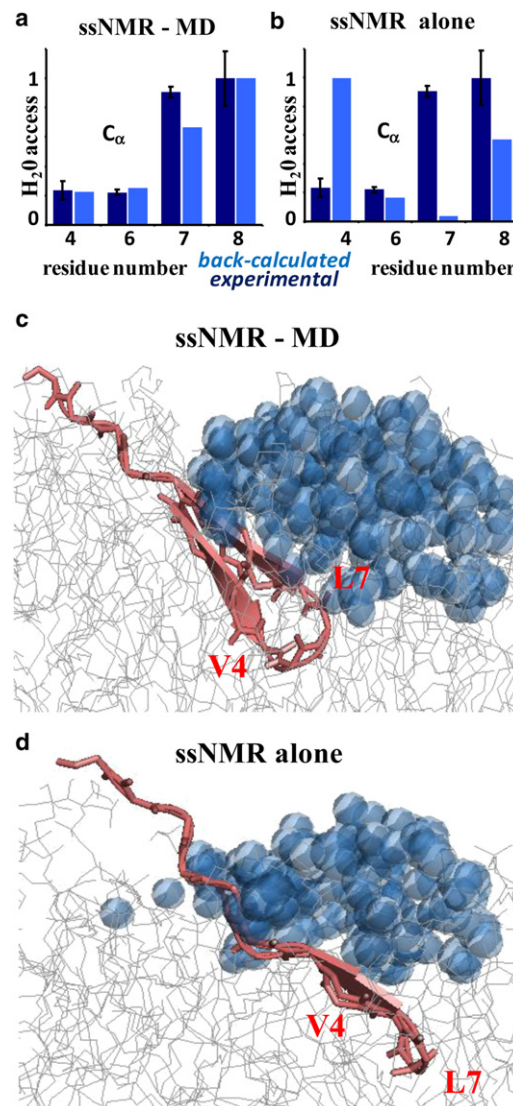


**FIGURE 4** Comparison of water access obtained with  $T_2$ -edited HHC experiments (dark blue columns) and back-calculated from MD simulations (light blue columns) for some resolved peptide  $C\alpha$ -positions. In a, the water access was back-calculated for the peptide structure and topology obtained by ssNMR-MD and in b for the (frozen) peptide structure and topology obtained by ssNMR alone. The number of water molecules was averaged within a radius of 9 Å from (a) 30–330 and (b) 5–10 ns MD trajectories. (c) SsNMR-MD and (d) ssNMR structure and topology. Water molecules within a radius of 6 Å around the  $C\alpha$  of A3-G9 are shown for clarity. See online version for colored figure versions.

the radius within which water molecules were averaged (Fig. S18). To verify the sensitivity of our approach, we carried out an additional simulation with a position restrained ssNMR structure and topology (Fig. 4 b). To this end, we assumed a rigid peptide structure while keeping the bilayer and the water flexible. Compared to the ssNMR topology, the ssNMR-MD arrangement was in much better agreement with the experimental data. Although the  $\beta$ -hairpin insertion depth and tilt of the  $\beta$ -hairpin with respect to the bilayer normal hardly changed over the course

of the simulations (see **Movie S1** in the Supporting Material), the  $\beta$ -hairpin plane significantly inclined so that the  $\beta$ -strand formed by residues 8–12 was oriented much closer to the water/lipid interface than for the ssNMR topology (**Fig. 4, c and d**). Notably, such an arrangement was in line with a reduced water access for V4 and G6, because the opposite  $\beta$ -strand is considerably further away from the water/lipid interface. One of the main reasons for the improved topology definition by our joint approach most likely is that the ssNMR structure was treated as a rigid body for the ssNMR topology determination, whereas MD simulations explore a much larger conformational space. Furthermore, we used a very simplified water/membrane interface for the ssNMR topology determination; whereas the MD simulation provides a better description of the complex membrane/water interface and also takes local bilayer distortions into account (see below).

To further investigate the peptide's orientational preferences, we performed a series of additional simulations with peptide insertion depths and orientations diverging from the ssNMR topology and back-calculated the water access for each topology. First, we observed that for all more deeply inserted peptides, with residues 1–12 well below the bilayer-water interface, the  $\beta$ -hairpin rapidly changed its tilt with respect to the membrane normal so that residues M1 and E12 stayed in close proximity to the bilayer-water interface, as concluded from the ssNMR data. The driving force for this reorientation is presumably charge-charge interactions involving the negatively charged carboxyl group of E12, the negatively charged lipid surface, and water molecules (**Fig. S19**). From these simulations, we can furthermore deduce that a small tilt (corresponding to  $\beta$ -strands almost aligned to the membrane normal) is not compatible with the experimentally probed water accessibility (**Fig. S20** and **Fig. S21, e and f**), because the water access of residues G6 and L7 would be considerably less than for residues V4 and Y8. Furthermore, very large tilt angles (corresponding to a  $\beta$ -hairpin sitting on the membrane surface) are only compatible if membrane and peptide planes are almost orthogonal to each other, otherwise the water access would be rather uniformly distributed (**Fig. S21 c**). This shows unambiguously that the correlation of experimental and simulated water access provides a sensitive means to test topological models of membrane-bound polypeptides. Notably, none of the topologies that deviated from the ssNMR findings converged to the ssNMR-MD topology after 30 ns of free simulation implying a huge influence of the starting structure and that the initial model derived from ssNMR alone was crucial.

## Supramolecular structure

The trajectory of the experimentally cross-validated and refined structure and topology subsequently served to investigate parameters that are experimentally difficult to assess,

including lipid-protein interactions. Whereas all polar backbone groups are saturated in  $\alpha$ -helical peptides, every second polar backbone group of a monomeric  $\beta$ -hairpin points toward the membrane, suggesting direct peptide-membrane interactions. First, the previously mentioned rotation of the  $\beta$ -hairpin plane brings residues Y8-E12 close to the water/membrane interface to allow for the formation of hydrogen bonds with water molecules or polar lipid groups. In contrast, hydrophobic residues M1-A5 on the opposite strand remain positioned close to the lipid chains. Remarkably, the  $\beta$ -hairpin features a slight twist (**Fig. 4 c** and **Fig. 5**), so as to simultaneously accommodate lipophilic (V4, L7) as well as bilayer/water (Y8-L10) interactions. Second, we observed a sharp decrease of the membrane width closely around the ShB peptide with several distorted lipid featuring phosphate and ester groups significantly deeper in the membrane than on average. Such local lipid arrangements enabled the backbone of M1, A2, G9, and even G6 and L7, which are rather deeply buried within the hydrophobic membrane core, to form intermolecular hydrogen bonds (**Fig. S22**). This is also in good accordance with a calorimetric study, which showed that phosphate groups coordinate to the membrane-bound ShB peptide (**72**). Note that the strong lipid interaction involving G6NH and L7NH (**Fig. S22**) may also explain why the back-calculated chemical shift of L7C $\alpha$  of the ssNMR-MD structure deviated from the experimental chemical shift, because such lipid-peptide contacts are not taken into account by current chemical-shift prediction algorithms. Finally, we observed cation- $\pi$  interaction between the aromatic ring of Y8 and sodium ions (**Fig. S23**). It is likely that such a cation- $\pi$  interaction modulates the

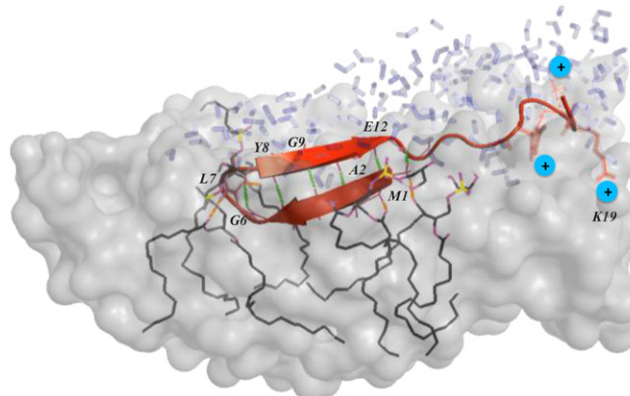


**FIGURE 5** Supramolecular structure of membrane-associated ShB peptide. The lipid bilayer surface is shown in gray, the peptide in red cartoon. Water molecules around peptide residues 1–12 within a radius of 9 Å are illustrated in blue. Hydrogen bonds between the  $\beta$ -strands and peptide-lipid hydrogen bonds are shown in green and orange, respectively. Distorted lipids (in gray lines) enable the formation of lipid-peptide hydrogen bonds. Interaction of the positively charged peptide tail with the negatively charged bilayer is illustrated. The snapshot was taken after 300 ns of the free simulation. See online version for colored figure versions.

chemical shift of all aromatic carbons, which can be a reason for the heterogeneity of the Y8 side chain (Fig. 1f).

In summary, the supramolecular structure (Fig. 5) of the membrane-bound ShB peptide is determined by the following intra- and intermolecular interactions (see also Movie S1 in the Supporting Material):

1. Intramolecular hydrogen bonds between the  $\beta$ -strands.
2. Intermolecular lipid headgroup- and lipid ester-peptide hydrogen bonds involving peptide residues close to the water/membrane interface. This is maximized in the ssNMR-MD arrangement featuring a twisted plane of the  $\beta$ -hairpin strongly inclined with respect to the membrane plane (Fig. 5). This positioning brings the strand formed by residues 8–12 very close to the water/lipid interface.
3. Intermolecular lipid headgroup-peptide hydrogen bonds between distorted lipids and the backbone of residues situated deeper within the membrane.
4. Hydrophobic interactions between side chains of residues 1–7 and the lipid chains, maximized by the twisted and inclined  $\beta$ -hairpin plane, which positions these hydrophobic residues close to the lipid chains (Fig. S24).
5. Anchoring of the peptide by the side chain of L7 in the hydrophobic membrane core (Fig. S25) (45,73).
6. The aromatic ring of Y8 alternating between hydrophobic interaction with L10 and cation- $\pi$  interaction with sodium ions (Fig. S23).
7. Transient electrostatic attraction between the positively charged tail of the ShB peptide (formed by residues 13–20) and negatively charged lipid headgroups (Fig. S4).

In addition, further MD studies indicated that dimeric membrane-bound ShB peptide constructs do not adopt  $\beta$ -hairpin structure, which suggests a monomeric membrane-binding mode of the ShB peptide (Fig. S26). This finding agrees well with fluorescence (44) and infrared (45) experiments and also is in line with studies of tetrameric K<sup>+</sup> channels, which demonstrated the ball-domains of each monomer to act mutually exclusive (74). Analogously, the membrane-bound ShB peptide is not subjected to oligomerization. Moreover, our data correlate with observations that the presence of negatively charged lipids (75) and negatively charged protein domains (76) distinctly affected gating of voltage-gated potassium channels by inactivating the N-terminal inactivating domain. With these findings, the supramolecular structure of membrane-bound ShB peptide offers new insights into N-type inactivation, particularly since recent studies corroborate  $\beta$ -sheet secondary structure for the channel-bound inactivation domain (73). Studying membrane-bound ShB peptide thus serves as a potential model to study N-type inactivation of potassium channels at an atomic level. Moreover, the fact that the ShB peptide adopts a stable  $\beta$ -hairpin in lipid bilayers may be a hint that ShB peptide membrane binding is

involved in the formation of the channel—ShB peptide complex.

## CONCLUSIONS

We have introduced a general approach to establish, refine, and validate the supramolecular structure of membrane-bound polypeptides using an iterative combination of MAS ssNMR spectroscopy and atomistic MD simulations. Notably, one uniformly (<sup>13</sup>C, <sup>15</sup>N) labeled sample suffices for our approach, neither requiring sample alignment nor site-specific labeling. This should render our approach particularly attractive for systems whose preparation is time-consuming or expensive. In addition, the error margin of our approach is low, because experimental and simulated data are cross-validated. Our approach is especially well suited for small membrane-associated peptides, often peripheral at the water/membrane interface, which play an important role in signal transduction and as potential drug targets (77). Altogether, the membrane-bound ShB peptide could be significantly better defined by the iterative joint approach than with one technique alone and our findings explain previous studies reporting global structural parameters for the membrane-bound ShB peptide (44,45). This demonstrates the potential of our approach for applications to a variety of membrane-bound systems underlining the high complementarity of ssNMR and MD for membrane-bound systems.

## SUPPORTING MATERIAL

Twenty-six figures, six tables, references, and a movie are available at [http://www.biophysj.org/biophysj/supplemental/S0006-3495\(12\)00569-3](http://www.biophysj.org/biophysj/supplemental/S0006-3495(12)00569-3).

We thank Ann-Kathrin Brückner for ShB peptide production, Gerhard Wolf for mass spectrometry analysis, and Karin Giller for liposome reconstitution preparations.

M.W. acknowledges financial support via a Federation of European Biochemical Societies (FEBS) Long-Term Fellowship. The research leading to these results has received funding from the European Community's Seventh Framework Programme (FP7/2007-2013) under grant agreement number 261863. This work was funded in part by the Deutsche Forschungsgemeinschaft (DFG; Ba 1700/9-1, Be 2345/5-1, Po 137/38-1) and the Netherlands Organisation for Scientific Research (A.M.J.J.B: grant 700.56.442; M.B: grants 700.26.121 and 700.10.443).

## REFERENCES

1. Ostermeier, C., and H. Michel. 1997. Crystallization of membrane proteins. *Curr. Opin. Struct. Biol.* 7:697–701.
2. Andrew, E. R., A. Bradbury, and R. G. Eades. 1958. Nuclear magnetic resonance spectra from a crystal rotated at high speed. *Nature*. 182: 1659–1659.
3. Reuther, G., K. T. Tan, ..., D. Huster. 2006. The lipidated membrane anchor of full length N-Ras protein shows an extensive dynamics as revealed by solid-state NMR spectroscopy. *J. Am. Chem. Soc.* 128: 13840–13846.

4. Hong, M. 2007. Structure, topology, and dynamics of membrane peptides and proteins from solid-state NMR spectroscopy. *J. Phys. Chem. B.* 111:10340–10351.
5. Ader, C., R. Schneider, ..., M. Baldus. 2007. Magic-angle-spinning NMR spectroscopy applied to small molecules and peptides in lipid bilayers. *Biochem. Soc. Trans.* 35:991–995.
6. Cady, S. D., K. Schmidt-Rohr, ..., M. Hong. 2010. Structure of the amantadine binding site of influenza M2 proton channels in lipid bilayers. *Nature.* 463:689–692.
7. Renault, M., M. P. Bos, ..., M. Baldus. 2011. Solid-state NMR on a large multidomain integral membrane protein: the outer membrane protein assembly factor BamA. *J. Am. Chem. Soc.* 133:4175–4177.
8. Yang, J., L. Aslimovska, and C. Glaubitz. 2011. Molecular dynamics of proteorhodopsin in lipid bilayers by solid-state NMR. *J. Am. Chem. Soc.* 133:4874–4881.
9. Ahmed, M. A., V. V. Bamm, ..., V. Ladizhansky. 2010. Solid-state NMR spectroscopy of membrane-associated myelin basic protein—conformation and dynamics of an immunodominant epitope. *Biophys. J.* 99:1247–1255.
10. Ader, C., R. Schneider, ..., M. Baldus. 2008. A structural link between inactivation and block of a K<sup>+</sup> channel. *Nat. Struct. Mol. Biol.* 15: 605–612.
11. Pfleger, N., A. C. Woerner, ..., C. Glaubitz. 2009. Solid-state NMR and functional studies on proteorhodopsin. *Biochem. Biophys. Acta.* 1787:697–705.
12. Andronesi, O. C., S. Becker, ..., M. Baldus. 2005. Determination of membrane protein structure and dynamics by magic-angle-spinning solid-state NMR spectroscopy. *J. Am. Chem. Soc.* 127:12965–12974.
13. Todokoro, Y., I. Yumen, ..., T. Fujiwara. 2006. Structure of tightly membrane-bound mastoparan-X, a G-protein-activating peptide, determined by solid-state NMR. *Biophys. J.* 91:1368–1379.
14. Cady, S. D., T. V. Mishanina, and M. Hong. 2009. Structure of amantadine-bound M2 transmembrane peptide of influenza A in lipid bilayers from magic-angle-spinning solid-state NMR: the role of Ser31 in amantadine binding. *J. Mol. Biol.* 385:1127–1141.
15. Hu, J., T. Asbury, ..., T. A. Cross. 2007. Backbone structure of the amantadine-blocked trans-membrane domain M2 proton channel from Influenza A virus. *Biophys. J.* 92:4335–4343.
16. Mani, R., M. Tang, ..., M. Hong. 2006. Membrane-bound dimer structure of a beta-hairpin antimicrobial peptide from rotational-echo double-resonance solid-state NMR. *Biochemistry.* 45:8341–8349.
17. Kumashiro, K. K., K. Schmidt-Rohr, ..., L. K. Thompson. 1998. A novel tool for probing membrane protein structure: solid-state NMR with proton spin diffusion and X-nucleus detection. *J. Am. Chem. Soc.* 120:5043–5051.
18. Ader, C., R. Schneider, ..., M. Baldus. 2009. Structural rearrangements of membrane proteins probed by water-edited solid-state NMR spectroscopy. *J. Am. Chem. Soc.* 131:170–176.
19. Luo, W. B., and M. Hong. 2010. Conformational changes of an ion channel detected through water-protein interactions using solid-state NMR spectroscopy. *J. Am. Chem. Soc.* 132:2378–2384.
20. Li, S., Y. Su, ..., M. Hong. 2010. Water-protein interactions of an arginine-rich membrane peptide in lipid bilayers investigated by solid-state nuclear magnetic resonance spectroscopy. *J. Phys. Chem. B.* 114:4063–4069.
21. Buffy, J. J., T. Hong, ..., M. Hong. 2003. Solid-state NMR investigation of the depth of insertion of protegrin-1 in lipid bilayers using paramagnetic Mn<sup>2+</sup>. *Biophys. J.* 85:2363–2373.
22. Li, C., M. Yi, ..., T. A. Cross. 2008. Solid-state NMR and MD simulations of the antiviral drug amantadine solubilized in DMPC bilayers. *Biophys. J.* 94:1295–1302.
23. Brown, L. S., L. C. Shi, ..., V. Ladizhansky. 2011. Conformation of a seven-helical transmembrane photosensor in the lipid environment. *Angew. Chem. Int. Ed.* 50:1302–1305.
24. van der Wel, P. C. A., E. Strandberg, ..., R. E. Koeppe. 2nd. 2002. Geometry and intrinsic tilt of a tryptophan-anchored transmembrane alpha-helix determined by (2)H NMR. *Biophys. J.* 83:1479–1488.
25. Strandberg, E., P. Wadhwan, ..., A. S. Ulrich. 2006. Solid-state NMR analysis of the PGLa peptide orientation in DMPC bilayers: structural fidelity of 2H-labels versus high sensitivity of 19F-NMR. *Biophys. J.* 90:1676–1686.
26. Wu, C. H., A. Ramamoorthy, and S. J. Opella. 1994. High-resolution heteronuclear dipolar solid-state NMR-spectroscopy. *J. Magn. Reson. A.* 109:270–272.
27. Ozdirekcan, S., C. Etchebest, ..., P. F. Fuchs. 2007. On the orientation of a designed transmembrane peptide: toward the right tilt angle? *J. Am. Chem. Soc.* 129:15174–15181.
28. Straus, S. K., W. R. Scott, and A. Watts. 2003. Assessing the effects of time and spatial averaging in 15N chemical shift/15N-1H dipolar correlation solid state NMR experiments. *J. Biomol. NMR.* 26:283–295.
29. Chandrasekhar, I., W. F. van Gunsteren, ..., B. H. Meier. 2006. Orientation and conformational preference of leucine-enkephalin at the surface of a hydrated dimyristoylphosphatidylcholine bilayer: NMR and MD simulation. *J. Am. Chem. Soc.* 128:159–170.
30. Kandasamy, S. K., D. K. Lee, ..., A. Ramamoorthy. 2009. Solid-state NMR and molecular dynamics simulations reveal the oligomeric ion-channels of TM2-GABA(A) stabilized by intermolecular hydrogen bonding. *Biochim. Biophys. Acta.* 1788:686–695.
31. Shi, L., A. Cembran, ..., G. Veglia. 2009. Tilt and azimuthal angles of a transmembrane peptide: a comparison between molecular dynamics calculations and solid-state NMR data of sarcolipin in lipid membranes. *Biophys. J.* 96:3648–3662.
32. Lam, Y. H., A. Hung, ..., A. Watts. 2010. Solid-state NMR and simulation studies of equinatoxin II N-terminus interaction with lipid bilayers. *Proteins.* 78:858–872.
33. Vogel, A., G. Reuther, ..., D. Huster. 2010. Backbone conformational flexibility of the lipid modified membrane anchor of the human N-Ras protein investigated by solid-state NMR and molecular dynamics simulation. *Biochim. Biophys. Acta.* 1798:275–285.
34. Holt, A., L. Rougier, ..., A. Milon. 2010. Order parameters of a transmembrane helix in a fluid bilayer: case study of a WALP peptide. *Biophys. J.* 98:1864–1872.
35. Ramamoorthy, A., S. K. Kandasamy, ..., R. G. Larson. 2007. Structure, topology, and tilt of cell-signaling peptides containing nuclear localization sequences in membrane bilayers determined by solid-state NMR and molecular dynamics simulation studies. *Biochemistry.* 46:965–975.
36. Esteban-Martín, S., E. Strandberg, ..., J. Salgado. 2009. Influence of whole-body dynamics on 15N PISEMA NMR spectra of membrane proteins: a theoretical analysis. *Biophys. J.* 96:3233–3241.
37. Bleile, D. W., W. R. Scott, and S. K. Straus. 2005. Can PISEMA experiments be used to extract structural parameters for mobile beta-barrels? *J. Biomol. NMR.* 32:101–111.
38. Vostrikov, V. V., B. A. Hall, ..., M. S. Sansom. 2010. Changes in transmembrane helix alignment by arginine residues revealed by solid-state NMR experiments and coarse-grained MD simulations. *J. Am. Chem. Soc.* 132:5803–5811.
39. Vogel, A., K. T. Tan, ..., D. Huster. 2007. Flexibility of ras lipid modifications studied by 2H solid-state NMR and molecular dynamics simulations. *Biophys. J.* 93:2697–2712.
40. Lange, A., Z. Gattin, ..., B. H. Meier. 2009. A combined solid-state NMR and MD characterization of the stability and dynamics of the HET-s(218–289) prion in its amyloid conformation. *ChemBioChem.* 10:1657–1665.
41. Allen, T. W., O. S. Andersen, and B. Roux. 2003. Structure of gramicidin a in a lipid bilayer environment determined using molecular dynamics simulations and solid-state NMR data. *J. Am. Chem. Soc.* 125:9868–9877.
42. Kurata, H. T., and D. Fedida. 2006. A structural interpretation of voltage-gated potassium channel inactivation. *Prog. Biophys. Mol. Biol.* 92:185–208.

43. Schott, M. K., C. Antz, ..., H. R. Kalbitzer. 1998. Structure of the inactivating gate from the *Shaker* voltage gated K<sup>+</sup> channel analyzed by NMR spectroscopy. *Eur. Biophys. J.* 27:99–104.
44. Encinar, J. A., A. M. Fernández, ..., J. M. González-Ros. 1998. Inactivating peptide of the *Shaker B* potassium channel: conformational preferences inferred from studies on simple model systems. *Biochem. J.* 331:497–504.
45. Poveda, J. A., M. Prieto, ..., C. R. Mateo. 2003. Intrinsic tyrosine fluorescence as a tool to study the interaction of the shaker B “ball” peptide with anionic membranes. *Biochemistry*. 42:7124–7132.
46. Encinar, J. A., A. M. Fernández, ..., J. M. Gonzalez-Ros. 2003. Probing the channel-bound *shaker B* inactivating peptide by stereoisomeric substitution at a strategic tyrosine residue. *Biochemistry*. 42:8879–8884.
47. Fung, B. M., A. K. Khitrin, and K. Ermolaev. 2000. An improved broadband decoupling sequence for liquid crystals and solids. *J. Magn. Reson.* 142:97–101.
48. Luca, S., D. V. Filippov, ..., M. Baldus. 2001. Secondary chemical shifts in immobilized peptides and proteins: a qualitative basis for structure refinement under magic angle spinning. *J. Biomol. NMR*. 20:325–331.
49. Baldus, M., A. T. Petkova, ..., R. G. Griffin. 1998. Cross polarization in the tilted frame: assignment and spectral simplification in heteronuclear spin systems. *Mol. Phys.* 95:1197–1207.
50. Seidel, K., A. Lange, ..., M. Baldus. 2004. Protein solid-state NMR resonance assignments from (C-13, C-13) correlation spectroscopy. *Phys. Chem. Chem. Phys.* 6:5090–5093.
51. Lange, A., S. Luca, and M. Baldus. 2002. Structural constraints from proton-mediated rare-spin correlation spectroscopy in rotating solids. *J. Am. Chem. Soc.* 124:9704–9705.
52. Weingarth, M., G. Bodenhausen, and P. Tekely. 2010. Broadband magnetization transfer using moderate radio-frequency fields for NMR with very high static fields and spinning speeds. *Chem. Phys. Lett.* 488:10–16.
53. Weingarth, M., P. Tekely, and G. Bodenhausen. 2008. Efficient heteronuclear decoupling by quenching rotary resonance in solid-state NMR. *Chem. Phys. Lett.* 466:247–251.
54. Brünger, A. T., P. D. Adams, ..., G. L. Warren. 1998. Crystallography & NMR system: a new software suite for macromolecular structure determination. *Acta Crystallogr. D Biol. Crystallogr.* 54:905–921.
55. Kukol, A. 2009. Lipid models for united-atom molecular dynamics simulations of proteins. *J. Chem. Theory Comput.* 5:615–626.
56. Hess, B., C. Kutzner, ..., E. Lindahl. 2008. GROMACS 4: algorithms for highly efficient, load-balanced, and scalable molecular simulation. *J. Chem. Theory Comput.* 4:435–447.
57. Soares, T. A., P. H. Hünenberger, ..., W. F. van Gunsteren. 2005. An improved nucleic acid parameter set for the GROMOS force field. *J. Comput. Chem.* 26:725–737.
58. Berger, O., O. Edholm, and F. Jähnig. 1997. Molecular dynamics simulations of a fluid bilayer of dipalmitoylphosphatidylcholine at full hydration, constant pressure, and constant temperature. *Biophys. J.* 72:2002–2013.
59. Kandt, C., W. L. Ash, and D. P. Tieleman. 2007. Setting up and running molecular dynamics simulations of membrane proteins. *Methods*. 41:475–488.
60. Bussi, G., D. Donadio, and M. Parrinello. 2007. Canonical sampling through velocity rescaling. *J. Chem. Phys.* 126:014101.
61. Borle, F., and J. Seelig. 1983. Structure of *Escherichia coli* membranes - deuterium magnetic-resonance studies of the phosphoglycerol head group in intact-cells and model membranes. *Biochemistry*. 22:5536–5544.
62. Hoover, W. G. 1985. Canonical dynamics: equilibrium phase-space distributions. *Phys. Rev. A*. 31:1695–1697.
63. Essmann, U., L. Perera, ..., L. G. Pedersen. 1995. A smooth particle mesh Ewald method. *J. Chem. Phys.* 103:8577–8593.
64. Hess, B., H. Bekker, ..., J. G. E. M. Fraaije. 1997. LINCS: a linear constraint solver for molecular simulations. *J. Comput. Chem.* 18: 1463–1472.
65. Baldus, M. 2006. Molecular interactions investigated by multi-dimensional solid-state NMR. *Curr. Opin. Struct. Biol.* 16:618–623.
66. Hutchinson, E. G., and J. M. Thornton. 1994. A revised set of potentials for beta-turn formation in proteins. *Protein Sci.* 3:2207–2216.
67. Seidel, K., M. Etzkorn, ..., M. Baldus. 2009. Comparative analysis of NMR chemical shift predictions for proteins in the solid phase. *Solid State Nucl. Magn. Reson.* 35:235–242.
68. Raleigh, D. P., M. H. Levitt, and R. G. Griffin. 1988. Rotational resonance in solid-state NMR. *Chem. Phys. Lett.* 146:71–76.
69. Weingarth, M., P. Tekely, ..., G. Bodenhausen. 2010. Improving the quality of 2D solid-state NMR spectra of microcrystalline proteins by covariance analysis. *Chem. Commun. (Camb.)*. 46:952–954.
70. Weingarth, M., Y. Masuda, ..., P. Tekely. 2011. Sensitive (13)C-(13)C correlation spectra of amyloid fibrils at very high spinning frequencies and magnetic fields. *J. Biomol. NMR*. 50:129–136.
71. Shen, Y., and A. Bax. 2010. SPARTA+: a modest improvement in empirical NMR chemical shift prediction by means of an artificial neural network. *J. Biomol. NMR*. 48:13–22.
72. Encinar, J. A., A. M. Fernandez, ..., J. M. Gonzalez-Ros. 1996. Interaction between ion channel-inactivating peptides and anionic phospholipid vesicles as model targets. *Biophys. J.* 71:1313–1323.
73. Molina, M. L., F. N. Barrera, ..., J. M. González-Ros. 2008. N-type inactivation of the potassium channel KcsA by the *Shaker B* “ball” peptide: mapping the inactivating peptide-binding epitope. *J. Biol. Chem.* 283:18076–18085.
74. Zagotta, W. N., T. Hoshi, and R. W. Aldrich. 1990. Restoration of inactivation in mutants of *Shaker* potassium channels by a peptide derived from ShB. *Science*. 250:568–571.
75. Oliver, D., C. C. Lien, ..., B. Fakler. 2004. Functional conversion between A-type and delayed rectifier K<sup>+</sup> channels by membrane lipids. *Science*. 304:265–270.
76. Roepke, J., S. Sewing, ..., O. Pongs. 1998. NIP domain prevents N-type inactivation in voltage-gated potassium channels. *Nature*. 391: 390–393.
77. Hickman, D. T., M. P. López-Deber, ..., A. Muhs. 2011. Sequence-independent control of peptide conformation in liposomal vaccines for targeting protein misfolding diseases. *J. Biol. Chem.* 286:13966–13976.